IEEE Access
Multidisciplinary | Rapid Review | Open Access Journal

Received June 29, 2020, accepted July 2, 2020, date of publication July 6, 2020, date of current version July 22, 2020.

Digital Object Identifier 10.1109/ACCESS.2020.3007494

Generation of High-Order Bessel Orbital Angular Momentum Vortex Beam Using a Single-Layer Reflective Metasurface

HAIXIA LIU, (Member, IEEE), HAO XUE, YONGJIE LIU, QIANG FENG, AND LONG LI, (Senior Member, IEEE)

Key Laboratory of High Speed Circuit Design and EMC, Ministry of Education, School of Electronic Engineering, Xidian University, Xi'an 710071, China

Corresponding author: Long Li (lilong@mail.xidian.edu.cn)

This work was supported in part by the Outstanding Young Foundation of Shaanxi Province of China under Contract 2019JC-15, and in part by the National Key Research and Development Program of China and Fundamental Research Funds JCKY2018203C025.

ABSTRACT In this paper, we propose a method to generate a high-order Bessel orbital angular momentum (OAM) vortex beam by using a single-layer reflective metasurface, which integrates the advantages of small size, high efficiency, insensitive polarization and stable incident angles. An offset-fed horn configuration is adopted to overcome the feed-blockage effect, and a subwavelength unit cell with rotational symmetry is designed to cover the reflection phase variation range of 360° in different incident angles. The metasurface is simulated, fabricated and measured at the center frequency of 10 GHz, and the results validate that a second-order Bessel OAM vortex beam can be generated effectively. By comparing the field distributions between the Bessel OAM vortex beam and the conventional OAM vortex beam, we find that the generated Bessel OAM vortex beam is obviously more convergent and has more stable field distributions. The single-layer reflective metasurface is simple and flexible to shape the wavefront to be a Bessel OAM vortex wave, which has the potential to be used in a wide range of applications.

INDEX TERMS Bessel orbital angular momentum (OAM) vortex beam, high efficiency, insensitive polarization, single-layer reflective metasurface, stable incident angles.

I. INTRODUCTION

Bessel beam has attracted much attention since Durnin solved it from the wave equation in 1987 [1]–[3]. The solution shows that the amplitude of the Bessel beam keeps unchanged as it propagates in free space, which has the potential to be used in wireless energy transmission and high-speed communications [4]–[6]. The high-order Bessel beam is called ''Bessel orbital angular momentum (OAM) vortex beam'' because it belongs to OAM beam, and its convergent characteristic has obvious advantages compared with divergent conventional OAM vortex beam. There have been many useful devices for generating or controlling conventional OAM vortex beam, like the single or array antenna [7]–[9], the metasurface [10]–[12], etc, but some of them are not suitable for Bessel OAM vortex beam [13]. Also, a finite size source can only generate pseudo-Bessel beam which possesses the nature as an ideal Bessel beam within a limited distance [14]–[19], so the methods and devices to generate high-performance Bessel beam are extremely challenging. There are some feasible methods proposed to generate high-order Bessel vortex beams in microwave bands, such as transmitarray [20]–[22] and reflective metasurface with polarizer [23]. However, when the electromagnetic energy passes through the dielectric, there will be some energy loss, which is not conducive to the conversion efficiency of energy. So that it is hard to resolve the contradiction between high efficiency and low profile [24], let alone small size. The characteristics about insensitive to polarization or incidence angles are also rarely realized simultaneously [11], which restricts a wide range of applications.

In this paper, a second-order Bessel OAM beam is generated by using a single-layer reflective metasurface with an offset-fed horn configuration at 10 GHz. As this configuration needs the unit cell to be miniaturized and less sensitivity to incidence angles, a subwavelength unit cell with the periodicity of 0.27λ(λ is wavelength in free space) is designed to meet the requirements. The unit cell leads to

The associate editor coordinating the review of this manuscript and approving it for publication was Weiren Zhu.

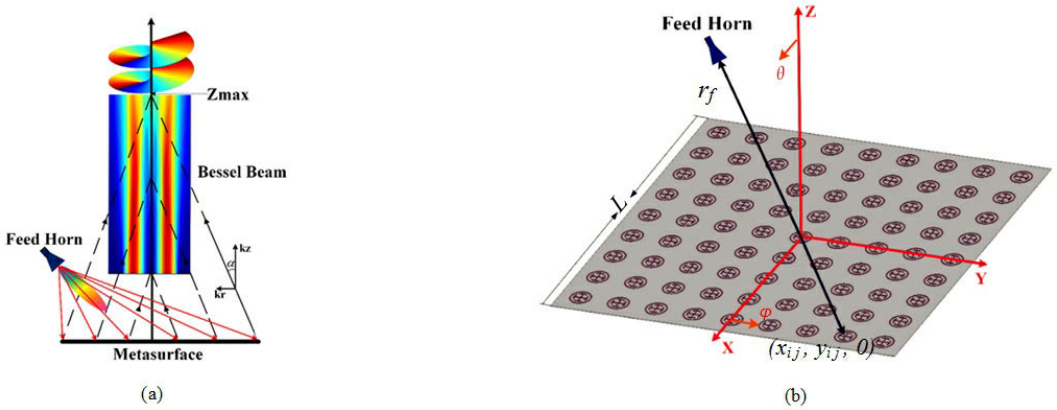

FIGURE 1. **(a) Principle illustration of the high-order Bessel beam generation using a reflective metasurface and (b) schematic diagram of the designed reflective metasurface and the coordinate configuration.**

the metasurface also has its mentioned advantages, while the whole device further has the characteristics of high efficiency and insensitive polarization. All of these beneficial characteristics making the metasurface has great flexibility in both fabrication and application, and the simulated and measured results validate that the high-performance second-order Bessel OAM vortex beam has been generated. For comparison, a conventional OAM vortex beam with the same order is designed and generated to illustrate the nondiffracting effect of the Bessel vortex beam. The results show that the Bessel OAM vortex beam has almost same transverse E-field intensity distributions in the nondiffracting region, which is more convenient to OAM vortex beams' reception and applications.

II. THEORY AND DESIGN METHODS

Using the method of variables separation to solve the Helmholtz equation in cylindrical coordinate system under the Sommerfeld radiation boundary condition, and considering the time harmonic factor $exp(j\omega t)$, we can obtain the complete solutions [25]:

$$E_{out}(r, \varphi, z) = H_n^{(1)}(k_r r)exp(-jk_z z + jn\varphi) \quad (1)$$

$$E_{in}(r, \varphi, z) = H_n^{(2)}(k_r r)exp(-jk_z z + jn\varphi) \quad (2)$$

where r is the radial coordinate, φ is the azimuthal angle coordinate, k_r and k_z are radial component and longitudinal component of the free space wavenumber k, i.e., $k = \sqrt{k_r^2 + k_z^2} = 2\pi/\lambda$. $H_n^{(1)}$ and $H_n^{(2)}$ represent the n^{th}-order first-kind Hankel function and second-kind Hankel function, respectively. Physical meaning of $H_n^{(1)}$ is a cylindrical travelling wave outward from z-axis in cylindrical coordinate system, while $H_n^{(2)}$ is a cylindrical travelling wave inward to z-axis. Therefore, the total wave vector k results in an outward (E_{out}) or an inward (E_{in}) conical wave. In addition, once the inward conical wave goes through z-axis, which will turn into an outward conical wave. It makes up of the foundation of only inward conical wave to generate Bessel beams [25]. If an inward conical wave and an outward conical wave exist simultaneously in the same spatial region, i.e., inward and outward conical waves are coherently superposed physically, the total E-field can be expressed as:

$$\begin{aligned} E_{total} &= E_{out}(r, \varphi, z) + E_{in}(r, \varphi, z) \\ &= 2J_n(k_r r)exp(-jk_z z + jn\varphi) \end{aligned} \quad (3)$$

This equation shows that Bessel beams of different orders can be formed in the overlapping region in various electromagnetic bands.

In Fig. 1(a), the operating mechanism of the Bessel beam generated by a reflective metasurface with a horn oblique incidence is illustrated. Based on the geometric optics theory, the angle between the inward conical waves or outward conical waves and z-axis is equal, i.e., $\tan\alpha = k_r/k_z$. The size of the radiant reflective metasurface determines the maximum distance $Z_{\max}$, which is the farthest overlapping region distance from the metasurface. It can be calculated by the following equation:

$$Z_{\max} = \frac{L}{2\tan\alpha} \quad (4)$$

where L is the dimension of the metasurface. The reflective metasurface transforms the spherical wave to the inward conical wave and it will become the outward conical wave after passing through the z-axis. Thus, the "Bessel beam area" is generated in the region where the inward and outward conical waves exist simultaneously.

The total compensation phase distribution for a high-order Bessel OAM vortex beam on the metasurface comprises three parts. The first part Φ_1 is the phase compensation from the feeding horn to the metasurface. Commonly, the feeding horn that is obliqued is placed at the position of $(r_f \sin\theta_f \cos\varphi_f, r_f \sin\theta_f \sin\varphi_f, r_f \cos\theta_f)$ in Cartesian coordinate system, and the position of any unit cell on the metasurface can be described as $(x_{ij}, y_{ij}, 0)$ at the coordinate system, as shown in Fig. 1(b). Then Φ_1 can be calculated by (5), as shown at the bottom of the next page. The second part Φ_2 is

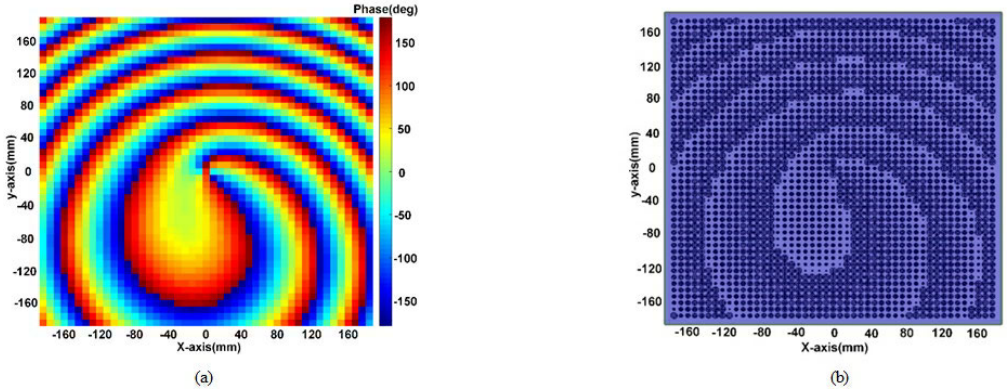

FIGURE 2. (a) Compensation phase distribution on the reflective metasurface to generate the second-order Bessel OAM vortex beam and (b) layout of the designed reflective metasurface with 47 × 47 elements.

the phase compensation that transforms the plane wave wave-front to the inward conical wave, which can be expressed as:

$$\Phi_2 = \frac{2\pi}{\lambda}\sqrt{x_{ij}^2 + y_{ij}^2}\sin(\alpha) \tag{6}$$

The third part of compensation phase that can generate the n^{th}-order Bessel OAM vortex beam's spiral phase is: $\Phi_3 = n\varphi_{ij} = n\arctan(y_{ij}/x_{ij})$. Based on these three parts, the total compensation phase distribution on the reflective metasurface is:

$$\Phi(x_{ij}, y_{ij}) = \Phi_1 + \Phi_2 + \Phi_3 \tag{7}$$

Based on the proposed approach, a single-layer reflective metasurface is designed, simulated and measured to generate a second-order Bessel OAM vortex beam. Considering the radial standing waves property of Bessel beams and the feed-blockage effect of reflective metasurfaces, an offset-fed horn configuration is adopted. The feeding horn parameters are set as: $r_f = 400, \theta_f = 20°, \varphi_f = 0°$, which means the feeding horn is located at (136.8mm, 0mm, 357.9mm) in the Cartesian coordinate system. The whole reflective metasurface is set to be composed of 47 × 47 elements with the dimension of 390mm×390mm (13λ × 13λ) at the operating frequency of 10GHz. According to Eq. (4), the maximal nondiffracting-distance $Z_{\max}$ is about 1100mm when the angle $\alpha = 10°$, then the compensation phase distribution of the designed metasurface in this case is calculated and shown in Fig. 2(a), which can shape the wave-front to be a second-order Bessel OAM vortex beam.

As the feeding horn is off-set, the incident angles actually vary from 0° up to 30° for different positions on the metasurface, so the unit cell needs to be less sensitivity to the incidence angles. As shown in Fig. 3, a subwavelength unit cell with the periodicity $P = 8.0$mm (0.27λ) is designed and printed on the F4B ($\varepsilon_r = 2.65$) dielectric substrate with

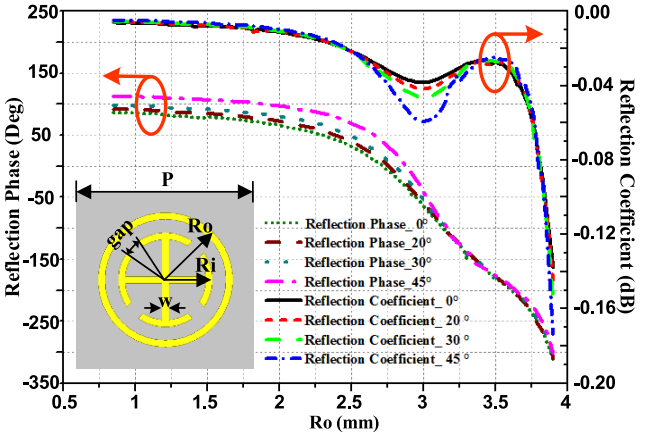

FIGURE 3. Geometry (top view) of the designed metasurface unit cell and the reflection phase and reflection coefficient versus the length of Ro in an infinite periodic model with different incident angles.

thickness t = 3.0mm. As the whole structure is symmetrical, this unit cell is both miniaturized and polarization-insensitive. The unit cell comprises two concentric circular rings, and the inner ring is separated by four identical gaps, while the separated four parts are also connected by a cross. The width of both the ring and the cross is w = 0.3mm, and the angles of the four identical gaps are 20°. The radiuses of the inner and outer ring are *Ri* and *Ro*, respectively, and the relationship between them can be expressed as: $Ri = 0.7 \times Ro$. By varying *Ro* from 0.85mm to 3.9mm, the reflection phase variation range of the unit cell can cover the whole 360° continuously, which is not easy to be achieved by only one structurally invariant unit cell [26]–[28]. Such large phase variation range is realized by the two parts of the unit cell: the first part is the combination of the separated inner ring and the cross, and the second part is the outer ring. If we observe the current distributions on

$$\Phi_1 = \frac{2\pi}{\lambda}\sqrt{\left(r_f \sin\theta_f \cos\varphi_f - x_{ij}\right)^2 + \left(r_f \sin\theta_f \sin\varphi_f - y_{ij}\right)^2 + \left(r_f \cos\theta_f\right)^2} \tag{5}$$

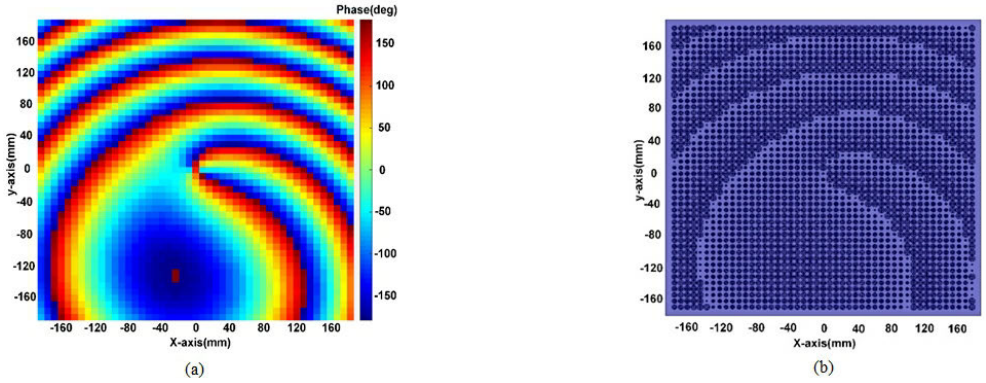

FIGURE 4. (a) Compensation phase distribution and (b) layout of the reflective metasurface for generating the conventional second-order OAM vortex beam.

the surface of the unit cell, it can be found that as the size of the unit cell becomes larger, the part with stronger intensity of surface current gradually changes from the second part to the first part. So that both of these two parts play a role in the reflection phase, thus achieving the phase variation range that neither of these two parts can achieve alone. As shown in Fig. 3, the reflection phase and reflection coefficient curves with different incidence angles (0°, 20°, 30°, and 45°) are presented. It can be seen that the phase-shift changes are less than 39.5° when the incidence angle varies from 0° to 45°, which shows a good angle stability. Meanwhile, the reflection coefficient keeps above -0.2 dB when the incidence angle varies, which shows not only the good angle stability, but also the characteristics of high efficiency that can contribute to the high efficiency of the metasurface. As the actual incidence angles for the metasurface unit cells vary from 0° to 30°, the variation range of the reflection phase is less than 17° according to Fig. 3, which is beneficial for the generation of high-order Bessel vortex beams.

Based on the designed unit cell, a single-layer reflective metasurface with 47 × 47 elements is designed to generate a second-order Bessel OAM vortex beam at 10 GHz. The total physical dimension of the designed metasurface is 390mm×390mm×3mm, and the layout of the designed reflective metasurface is shown in Fig. 2(b). As the metasurface is composed of unit cells, whose sizes are calculated based on their relationship with the reflection phases, the distribution of them corresponds to the compensation phase distribution. Then the metasurface is simulated by the full-wave electromagnetic simulation software (ANSYS HFSS), and a standard X-band horn antenna is used as the feeding source. To illustrate the effect of non-diffraction transmission, a reflective metasurface is designed to generate a conventional second-order OAM vortex beam based on the previous methods [29]–[31]. Comparing with the designed Bessel OAM vortex beam, the conventional OAM vortex beam generated by a reflective metasurface with the same dimension does not exist the transverse k vector. So that the compensation phase distribution and the layout of the reflective metasurface for the designed conventional OAM beam are different from those of Bessel OAM vortex beam shown in Fig. 2, and the corresponding figures are shown in Figs. 4(a) and 4(b), respectively.

III. RESULTS AND DISCUSSION

A. SIMULATION RESULTS AND DISCUSSION

The performance comparisons between the Bessel OAM vortex beam and the conventional OAM beam are shown in Fig. 5. It can be seen that the second-order Bessel OAM vortex beam is successfully generated. The simulated normalized E-field amplitude distribution of the second-order Bessel vortex beam in xoz-plane is shown in Fig. 5(a), and the normalized E-field amplitude and E-field phase distributions in xoy-plane are shown on observational planes with a size of 0.8m×0.8m. There are three observational planes locating at the distances of 20 wavelengths (600mm), 30 wavelengths (900mm) and 36.7 wavelengths (1100mm) away from the Bessel metasurface, and the simulated results are shown in Figs. 5(b) and 5(c), respectively. For comparison, the conventional OAM vortex beam performances are shown in Figs. 5(d), 5(e) and 5(f) under the same conditions. It can be seen that the E-field amplitude distributions in xoz-plane of the generated Bessel OAM vortex beam are kept almost unchanged in ''Bessel nondiffracting area''. By comparing with the amplitude and phase distributions in xoy-plane of the two beams, it can be seen that the field distributions of the Bessel OAM vortex beams are more stable than those of the conventional OAM vortex beams. These characteristics make the Bessel OAM vortex beam easier to be received and applied within the ''Bessel nondiffracting area''.

As the generation of Bessel OAM vortex beam is achieved, the advantages of small size, insensitive polarization and stable incident angles of our device are also verified. The efficiencies of the Bessel OAM beam can also be simulated on the mentioned observational planes to be 56.1%, 45.9%, and 40.3%, respectively, which shows a really high efficiency for the Bessel OAM vortex beam. It's worth mentioning

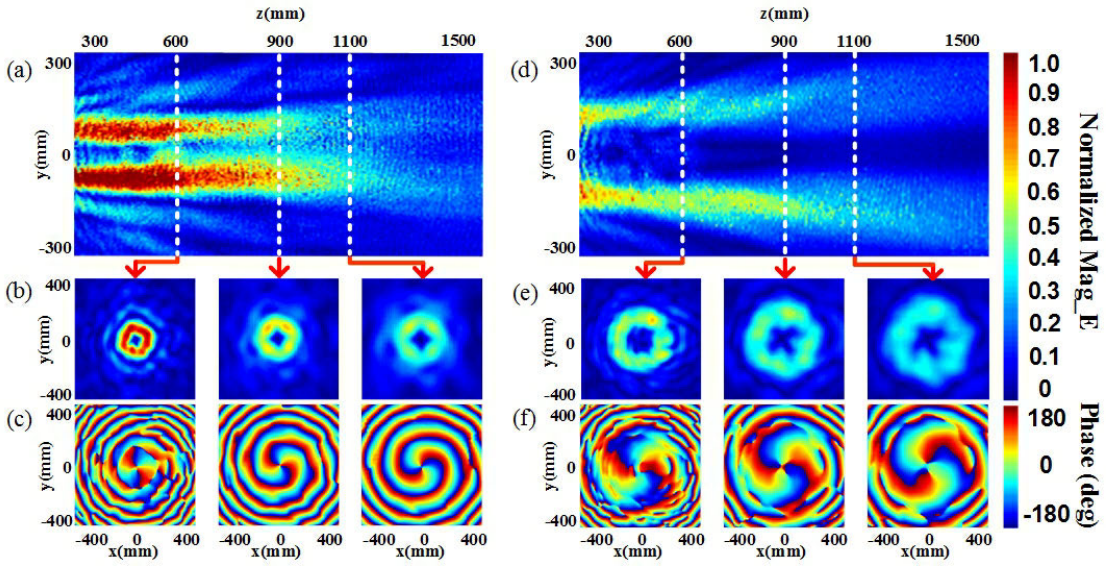

FIGURE 5. Comparison of the second-order Bessel OAM vortex beam and the second-order conventional OAM vortex beam. (a) Normalized E-field amplitude of Bessel OAM vortex beam in xoz-plane, (b) normalized E-field amplitude distributions and (c) E-field phase distributions on the different observational planes at the location of 600mm, 900mm and 1100mm away from the reflective Bessel metasurface, (d) normalized E-field amplitude of conventional OAM vertex beam in xoz-plane, (e) normalized E-field amplitude distributions and (f) E-field phase distributions on the different observational planes at the location of 600mm, 900mm and 1100mm away from the reflective conventional metasurface.

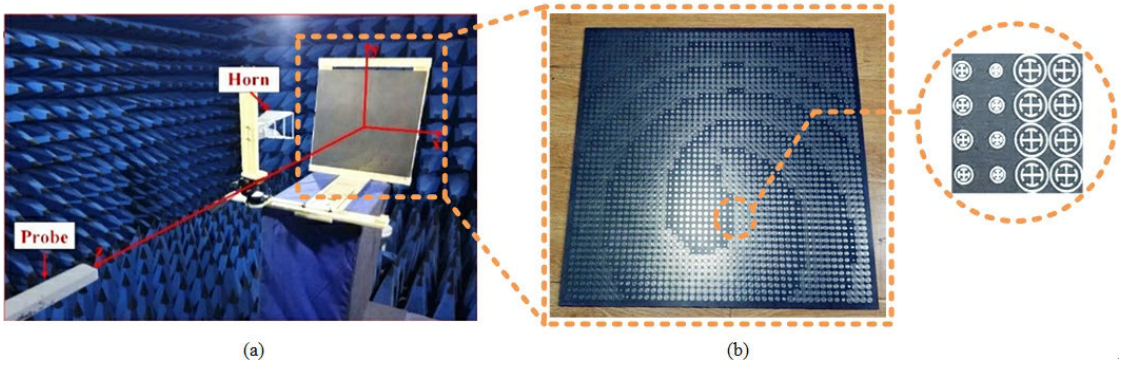

FIGURE 6. (a) Experimental system configuration for the Bessel vortex beam measurement and (b) prototype of the fabricated reflective metasurface.

that the efficiency is calculated by the comparison with the whole energy from the feeding horn, and we choose these observational planes which are far from the metasurface to avoid the effect of the feeding horn.

B. MEASUREMENT RESULTS AND DISCUSSION

The nondiffracting effect of the Bessel vortex beam is well verified and the reflective metasurface is fabricated and measured. It was measured by using near-filed planar-scanning techniques at 10 GHz to further validate the results of our design. The prototype of the reflective metasurface and the near-filed measurement environment in the anechoic chamber are shown in Fig. 6. A standard waveguide probe is used to detect the corresponding electric field distribution. The size of the scanning plane is 0.6m×0.6m and the measured lattice length of the sampling grid is 10mm.

The normalized E-field amplitude and the E-field phase distributions are measured on different observational planes, which are 600mm, 900mm, and 1100mm away from the reflective metasurface, as shown in Figs. 7 (b) and 7(d), respectively. For comparison, the simulated results are also shown in Figs. 7(a) and 7(c), respectively. The measured doughnut-shaped E-field amplitude distribution and spiral phase distribution that varies from 0 to 2π with two turns show that the second-order Bessel-like vortex beam has been generated. It can be seen that the measured results are in good agreement with the simulated results.

In order to further examine the nondiffracting characteristic of the Bessel beam, we can discuss the full width at

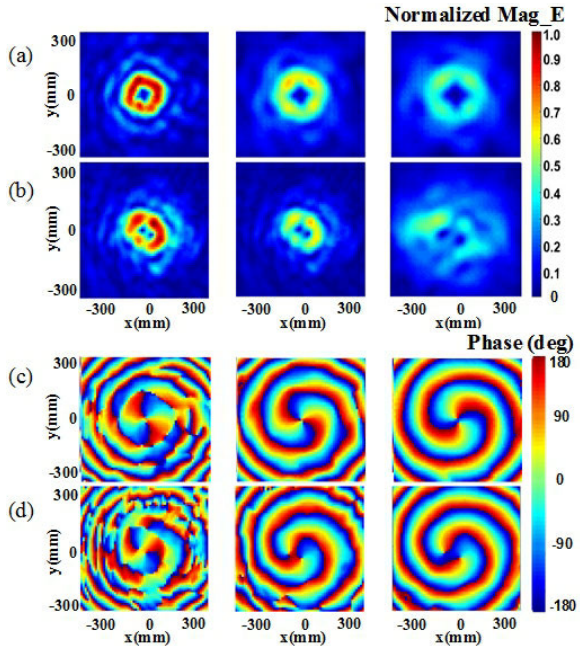

FIGURE 7. Comparison of the measured results and the simulated results of E-field distributions of the generated second-order Bessel vortex beam on the different observational planes. (a) Simulated normalized E-field amplitude distributions, (b) measured normalized E-field amplitude distributions, (c) simulated E-field phase distributions, and (d) measured E-field phase distributions.

half maximum (FWHM) value of Bessel beam, which means twice the distance from the center dark spot to the closest point on the ring at the half of the maximum intensity. According to the definition and equation of the FWHM [22], it is easy to find that the theoretical value of the Bessel beam generated is 62mm. Then the simulated values can be gotten as 76mm and 72mm based on the data of E-field on the observational planes at the location of 600mm and 900mm away from the reflective Bessel metasurface. And the corresponding measured values are 64mm and 78mm, respectively. We choose these observational planes which are neither too close nor too far from the metasurface to avoid the effect of the feeding horn and the effect of the reduced energy. It can be seen that the simulated and measured values are in good agreement with the theoretical one. There are some acceptable errors between the simulated values and the measured values, this is because the actual measurement environment and measurement errors are bound to have some effect on the generated beam. As a result, the measured E-field amplitude distributions on the observation planes are deteriorative compared with the simulated one, and the reduction in sampling points also exacerbates this effect. At the same time, as the values on different observational planes are close to each other in the nondiffracting area, it is a good illustration of the nondiffracting characteristics of the Bessel beam generated.

IV. CONCLUSION

In this paper, we proposed a single-layer reflective metasurface based on the subwavelength unit cell and the off-set feeding source to generate the second-order Bessel OAM vortex beam. The reflective metasurface can be feasibly applied to launch high-order non-diffractive Bessel-like beams carrying OAM. The simulated and measured results show that the generated Bessel vortex beam is non-diffracting in a limited region. It is worth pointing out that the designed Bessel beam launcher with high efficiency is simple, polarization-insensitive, and insensitive to incidence angles, which could be used to generate multiple Bessel OAM vortex beams in a wide range of applications.

ACKNOWLEDGMENT

(*Haixia Liu and Hao Xue contributed equally to this work.*)

REFERENCES

[1] J. Durnin, "Exact solutions for nondiffracting beams. I. The scalar theory," *J. Opt. Soc. Amer. A, Opt. Image Sci.*, vol. 4, no. 4, pp. 651–654, 1987.
[2] J. Arlt and K. Dholakia, "Generation of high-order Bessel beams by use of an axicon," *Opt. Commun.*, vol. 177, nos. 1–6, pp. 297–301, Apr. 2000.
[3] E. Stankevičius, M. Garliauskas, M. Gedvilas, and G. Račiukaitis, "Bessel-like beam array formation by periodical arrangement of the polymeric round-tip microstructures," *Opt. Express*, vol. 23, no. 22, pp. 28557–28566, 2015.
[4] Y. B. Li, B. G. Cai, X. Wan, and T. J. Cui, "Diffraction-free surface waves by metasurfaces," *Opt. Lett.*, vol. 39, no. 20, pp. 5888–5891, 2014.
[5] A. Mazzinghi, M. Balma, D. Devona, G. Guarnieri, G. Mauriello, M. Albani, and A. Freni, "Large depth of field pseudo-Bessel beam generation with a RLSA antenna," *IEEE Trans. Antennas Propag.*, vol. 62, no. 8, pp. 3911–3919, Aug. 2014.
[6] E. S. Gamez Rodriguez, M. Machnoor, and G. Lazzi, "On the generation of nondiffracting beams in extremely subwavelength applications," *IEEE Trans. Antennas Propag.*, vol. 65, no. 10, pp. 5228–5237, Oct. 2017.
[7] M. Barbuto, F. Trotta, F. Bilotti, and A. Toscano, "Circular polarized patch antenna generating orbital angular momentum," *Prog. Electromagn. Res.*, vol. 148, pp. 23–30, 2014.
[8] H. Xue, H. Liu, Q. Shao, Q. Feng, and L. Li, "Double-deflection vortex beams generation using a single elliptical patch with the theory of characteristic modes," *Opt. Express*, vol. 28, no. 8, pp. 12322–12330, 2020.
[9] S. Mohaghegh Mohammadi, L. K. S. Daldorff, J. E. S. Bergman, R. L. Karlsson, B. Thide, K. Forozesh, T. D. Carozzi, and B. Isham, "Orbital angular momentum in radio—A system study," *IEEE Trans. Antennas Propag.*, vol. 58, no. 2, pp. 565–572, Feb. 2010.
[10] X. Bai, A. Cao, F. Kong, J. Qian, S. Xu, W. Yan, C. He, X. Liang, R. Jin, and W. Zhu, "Rotman lens-fed Fabry–Pérot resonator antennas for generating converged multi-mode OAM beams," *IEEE Access*, vol. 7, pp. 105768–105775, 2019.
[11] X. Bai, F. Kong, J. Qian, Y. Song, C. He, X. Liang, R. Jin, and W. Zhu, "Polarization-insensitive metasurface lens for efficient generation of convergent OAM beams," *IEEE Antennas Wireless Propag. Lett.*, vol. 18, no. 12, pp. 2696–2700, Dec. 2019.
[12] J. Han, L. Li, H. Yi, and Y. Shi, "1-Bit digital orbital angular momentum vortex beam generator based on a coding reflective metasurface," *Opt. Mater. Express*, vol. 8, no. 11, pp. 3470–3478, 2018.
[13] P. Lemaitre-Auger, S. Abielmona, and C. Caloz, "Generation of Bessel beams by two-dimensional antenna arrays using sub-sampled distributions," *IEEE Trans. Antennas Propag.*, vol. 61, no. 4, pp. 1838–1849, Apr. 2013.
[14] Z. Li, K. B. Alici, H. Caglayan, and E. Ozbay, "Generation of an axially asymmetric Bessel-like beam from a metallic subwavelength aperture," *Phys. Rev. Lett.*, vol. 102, no. 14, Apr. 2009, Art. no. 143901.
[15] M. Qing Qi, W. X. Tang, and T. J. Cui, "A broadband Bessel beam launcher using metamaterial lens," *Sci. Rep.*, vol. 5, no. 1, Dec. 2015, Art. no. 011732.
[16] J. Turunen, A. Vasara, and A. T. Friberg, "Holographic generation of diffraction-free beams," *Appl. Opt.*, vol. 27, no. 19, pp. 3959–3962, 1988.
[17] O. Brzobohatý, T. Čižmár, and P. Zemánek, "High quality quasi-Bessel beam generated by round-tip axicon," *Opt. Express*, vol. 16, no. 17, pp. 12688–12700, 2008.

[18] M. Ettorre and A. Grbic, "Generation of propagating Bessel beams using leaky-wave modes," *IEEE Trans. Antennas Propag.*, vol. 60, no. 8, pp. 3605–3613, Aug. 2012.
[19] J. Durnin, J. J. Miceli, Jr., and J. H. Eberly, "Diffraction-free beams," *Phys. Rev. Lett.*, vol. 58, pp. 1499–1501, Apr. 1987.
[20] N. Kou, S. Yu, and L. Li, "Generation of high-order Bessel vortex beam carrying orbital angular momentum using multilayer amplitude-phase-modulated surfaces in radiofrequency domain," *Appl. Phys. Express*, vol. 10, no. 1, Jan. 2017, Art. no. 016701.
[21] K. Zhang, Y. Yuan, D. Zhang, X. Ding, B. Ratni, S. N. Burokur, M. Lu, K. Tang, and Q. Wu, "Phase-engineered metalenses to generate converging and non-diffractive vortex beam carrying orbital angular momentum in microwave region," *Opt. Express*, vol. 26, no. 2, pp. 1351–1360, Jan. 2018.
[22] M. R. Akram, M. Q. Mehmood, T. Tauqeer, A. S. Rana, I. D. Rukhlenko, and W. Zhu, "Highly efficient generation of Bessel beams with polarization insensitive metasurfaces," *Opt. Express*, vol. 27, no. 7, p. 9467, 2019.
[23] Y. Shen, J. Yang, H. Meng, W. Dou, and S. Hu, "Generating millimeter-wave Bessel beam with orbital angular momentum using reflective-type metasurface inherently integrated with source," *Appl. Phys. Lett.*, vol. 112, no. 14, Apr. 2018, Art. no. 141901.
[24] M. Khorasaninejad, A. Y. Zhu, C. Roques-Carmes, W. T. Chen, J. Oh, I. Mishra, R. C. Devlin, and F. Capasso, "Polarization-insensitive metalenses at visible wavelengths," *Nano Lett.*, vol. 16, no. 11, pp. 7229–7234, Nov. 2016.
[25] S. Chavez-cerda, "A new approach to Bessel beams," *J. Modern Opt.*, vol. 46, no. 6, pp. 923–930, May 1999.
[26] P. Su, Y. Zhao, S. Jia, W. Shi, and H. Wang, "An ultra-wideband and polarization-independent metasurface for RCS reduction," *Sci. Rep.*, vol. 6, no. 1, p. 20387, Apr. 2016.
[27] Q. Zheng, Y. Li, J. Zhang, H. Ma, J. Wang, Y. Pang, Y. Han, S. Sui, Y. Shen, H. Chen, and S. Qu, "Wideband, wide-angle coding phase gradient metasurfaces based on pancharatnam-berry phase," *Sci. Rep.*, vol. 7, no. 1, p. 43543, Apr. 2017.
[28] J. Li, Z. Zhao, and J. Yao, "Flexible manipulation of terahertz wave reflection using polarization insensitive coding metasurfaces," *Opt. Express*, vol. 25, no. 24, pp. 29983–29992, 2017.
[29] F. Bayatpur and K. Sarabandi, "Single-layer high-order miniaturized-element frequency-selective surfaces," *IEEE Trans. Microw. Theory Techn.*, vol. 56, no. 4, pp. 774–781, Apr. 2008.
[30] S. Yu, L. Li, G. Shi, C. Zhu, X. Zhou, and Y. Shi, "Design, fabrication, and measurement of reflective metasurface for orbital angular momentum vortex wave in radio frequency domain," *Appl. Phys. Lett.*, vol. 108, no. 12, Mar. 2016, Art. no. 121903.
[31] S. Yu, L. Li, G. Shi, C. Zhu, and Y. Shi, "Generating multiple orbital angular momentum vortex beams using a metasurface in radio frequency domain," *Appl. Phys. Lett.*, vol. 108, no. 24, Jun. 2016, Art. no. 241901.

HAIXIA LIU (Member, IEEE) received the B.S. and M.S. degrees in test and measurement technique and instrumentation and the Ph.D. degree in electromagnetic fields and microwave technology from Xidian University, Xi'an, China, in 1998, 2001, and 2014, respectively.

She studied as a Cooperative Graduate at Shizuoka University, Shizuoka, Japan, in 2001. Since 2002, she has been working with Xidian University. Her research interests include circuit analysis, frequency measurement and control, wireless power transfer, antennas, and electromagnetic compatibility.

HAO XUE was born in Shaanxi, China. He received the B.E. degree in electronic and information engineering from Xidian University, Xi'an, China, in 2015, where he is currently pursuing the Ph.D. degree in electronic science and technology. His research interests include antenna design, metasurface, characteristic mode theory, and OAM vortex beam. He received the honors and awards include the National Scholarship for Postgraduates 2017 and the Best Student Paper Award of the IEEE iWAT 2018.

YONGJIE LIU was born in Guizhou, China. He received the B.E. degree in electronic and information engineering and the M.E. degree in electromagnetic fields and microwave technology from Xidian University, Xi'an, China, in 2016 and 2019, respectively. His research interests include antennas, metasurface, nondiffracting beam, and OAM vortex beam.

QIANG FENG was born in Shanxi, China, in 1992. He received the B.E. degree in electromagnetic wave propagation and antenna from Xidian University, Xi'an, China, in 2015, where he is currently pursuing the Ph.D. degree in electromagnetic field and microwave technology with the School of Electronic Engineering. His current research interests include metasurface, antenna arrays, and the application of radio OAM vortex wave.

LONG LI (Senior Member, IEEE) received the B.E. and Ph.D. degrees in electromagnetic fields and microwave technology from Xidian University, Xi'an, China, in 1998 and 2005, respectively.

He was a Senior Research Associate with the Wireless Communications Research Center, City University of Hong Kong, in 2006. From 2006 to 2008, he was a JSPS Fellow with Tohoku University, Sendai, Japan. He was a Senior Visiting Scholar with Pennsylvania State University, USA, in 2014. He is currently a Professor with the School of Electronic Engineering, Xidian University. He is also the Director of the Key Laboratory of High-Speed Circuit Design and EMC, Ministry of Education, China. He is also the Dean of the Hai-Tang No.9 Academy, Xidian University. He has authored or coauthored over 100 articles in journals. He holds more than 20 patents. His research interests include metamaterials/ metasurfaces, antennas and microwave devices, field-circuit collaborative design and EMC, wireless power transfer and harvesting technology, and OAM vortex waves.

Dr. Li is a Senior Member of CIE. He received the Nomination Award of National Excellent Doctoral Dissertation of China, in 2007, the Best Paper Award in the International Symposium on Antennas and Propagation, in 2008, the Program for New Century Excellent Talents in University of the Ministry of Education of China, in 2010, the First Prize of Awards for Scientific Research Results offered by Shaanxi Provincial Department of Education, China, in 2013, the IEEE APS Raj Mittra Travel Grant Senior Researcher Award, in 2015, the Shaanxi Youth Science and Technology Award, in 2016, the Outstanding Young Foundation of Shaanxi Province of China, and the Japan Society for Promotion of Science (JSPS) Postdoctoral Fellowship. He is the Vice-President of MTT-Chapter in IEEE Xi'an Section. He is a TPC Co-Chair of APCAP2017 and a General Co-Chair of AWPT2019. He serves as an Associate Editor for *ACES Journal* and a Guest Editor of the IEEE J-ERM Special Issue.